Characterization of $Li_2MoO_4/BaTiO_3$ All-Ceramic Films on Organic Substrate Printed Capacitors at 45 MHz–10 GHz

S. Myllymäki, M. Väätäjä, G. Omodara, H. Kähäri, J. Juuti, and H. Jantunen

***Abstract*— This article presents novel all-ceramic composite films used as a screen-printed capacitors on polymer surface and their characterization at 45-MHz to 10-GHz frequency range. All-ceramic composite paste is based on lithium molybdate (Li_2MoO_4), barium titanate ($BaTiO_3$), and water manufactured by the room temperature fabrication (RTF) method. For the determination of the permittivity and the loss tangent of the materials, ceramic thick films are printed on the top of an interdigital-shaped microwave capacitors using pastes with 0, 10, and 20 vol.% of $BaTiO_3$ filler in Li_2MoO_4 followed by a drying process at 120 °C. The electrical properties of the capacitors, capacitance, and quality value are derived from measured *S*-parameter results, whereas the electrical properties of the ceramic thick-film materials, real, and imaginary values of permittivity are derived from the measured results through computer simulations. The electrical properties of the ceramic material, such as moderate permittivity and moderately low-loss tangent, could be adjusted by changing the volume fraction of the $BaTiO_3$ filler to match the demands of different areas of applications. The obtained results are verified with five samples of each ceramic composition. The results show the capacitance values of 0.30 pF for an uncoated capacitor and 0.55, 0.67, and 0.95 pF with coatings of Li_2MoO_4 with 0, 10, and 20 vol.% of $BaTiO_3$ composites, respectively, at 2.5-GHz frequency. The calculated relative permittivity (ε_r) values for the same materials are 3.70, 5.23, and 6.43, and loss tangent values are 0.035, 0.027, and 0.036 at 2.5 GHz. These novel all-ceramic capacitor composite materials are applicable for the RF components used in telecommunication applications in the frequency range of 45 MHz–10 GHz, thus widening the technology roadmap in terms of material choices for different applications, especially high thermal resistant materials.**

***Index Terms*— All-ceramic, barium titanate ($BaTiO_3$), composites, lithium molybdate (Li_2MoO_4), microwave, printed interdigital capacitor, RF passives, room temperature fabrication (RTF), screen printing.**

Manuscript received March 23, 2021; accepted January 30, 2022. Date of publication March 8, 2022; date of current version May 2, 2022. This work was supported in part by the European Research Council (ERC) through the European Union's Seventh Framework Program (FP7/2007–2013)/ERC under Agreement 291132, in part by ERC POC under Project 812837, in part by the Academy of Finland Research Infrastructure "Printed Intelligence Infrastructure" (PII-FIRI) under Grant 320017, and in part by the Academy of Finland 6Genesis Flagship under Grant 318927. *(Corresponding author: S. Myllymäki.)*

The authors are with the Microeletronics Research Unit, University of Oulu, 90014 Oulu, Finland (e-mail: sami.myllymaki@oulu.fi).

Color versions of one or more figures in this article are available at https://doi.org/10.1109/TDEI.2022.3157913.

Digital Object Identifier 10.1109/TDEI.2022.3157913

I. Introduction

THE printed electronics technology is known from features of large area, low cost, sustainable, scalable, intelligent, robust, power efficient, thin, and lightweight solutions that has been developed lately to provide conformable and stretchable characteristics as well [1]. Low-temperature inorganic material processing will be an essential part of sustainability that is the key feature required for future manufacturing. Thus, additive technologies and adjustable material properties demonstrate an efficient way to utilize nature's resources. In addition, flexible hybrid electronics combines silicon technologies, e.g., ICs with organic printed electronics technologies. This enables the technology to be used for a wide range of applications, such as printed sensors, thinned silicon ICs, printed antennas, energy harvesting modules, and displays. In addition, wearable and structural health, industrial and environmental sensors have been applied [2]. However, in case of wider range of inorganic materials, like ceramics, the associated high-temperature sintering or sputtering methods limit their practical application to flexible organic substrates. Thus, methods to fabricate such materials at low temperature with useful electrical properties are needed.

To realize these systems, it is necessary to develop printable materials with low losses and adequate permittivity values, especially for high-frequency applications [3]. Polymer-based functional composite materials with a suitable low-loss and high relative permittivity already exist [4]–[6]. PMMA/$BaTiO_3$ composites in [4], for example, have a relative permittivity between 25 and 32 and loss tangents between 0.02 and 0.06 in the 0.5–3-GHz frequency range. Chameswary and Sebastian [5] reported the dielectric properties of a $BaTiO_3$ filled butyl rubber composites processed at a temperature of 200 °C. The composites exhibited a relative permittivity of 3.5 and loss tangent of 0.005 with 10 vol.% content, and a relative permittivity of 8 and loss tangent of 0.02 with 30 vol.% content at 5-GHz frequency. Wang *et al.* [7] prepared polyimide/$BaTiO_3$ composites with different contents from 0 to 90 wt.% (0–67.5 vol.%), which yielded a relative permittivity ranging from 3.53 to 46.50 and loss tangent from 0.005 to 0.015 at a frequency of 10 kHz. Similar results were also reported in [8].

Recently, thick films of all-ceramic composites have been investigated for printed electronics technology. Ceramic materials earlier known for high-temperature processing are now

meeting low-processing temperature similar to polymer composites and thus widening the technology roadmap of the heterogeneous integration and adjustable dielectrics [9]. The functional ceramic particles were distributed inside the ceramic matrix enabling easy processing at relatively low temperatures [10]–[12]. All-ceramic composites are resistant for high operation temperatures, such as 120 °C or 525 °C, in the electronics packages. The room temperature fabrication (RTF) method, offering the means for low-temperature ceramics processing without the use of organic materials or high-temperature sintering, has previously been introduced for bulk structures. The RTF method relies on the water solubility of a ceramic material to form an aqueous phase that aids the packing of the solid ceramic particles during the press processing. The ceramic material used in RTF is lithium molybdate (Li_2MoO_4), a nontoxic dielectric material with a low relative permittivity (ε_r) 5.1 and loss tangent ($\tan\delta$) 0.0004 at 9.6 GHz [10].

Material permittivity and permeability measurements are essential for an accurate design process in many applications. Assuring this, there are widely used techniques for the microwave region, such as the methods based on the cavity resonator, Fabry–Perot resonators, free space, open-ended coaxial probe, and transmission lines [13]–[17]. Typically, resonator methods are accurate and narrowband, whereas the free-space and open-ended coaxial probe methods operate over a wideband but are less accurate. The transmission-line techniques are the most popular methods for electromagnetic characterization in wideband frequencies. However, because they include short and open lines and transmission/reflection lines standards, they are still limited by the tolerances of the contact resistances and the fabrication.

In this article, high-frequency interdigital capacitors were selected as a demonstrative electrical application utilizing the RTF technology for the first time to create capacitor structures utilizing screen-printed capacitors of the all-ceramic composite thick films onto silver conductors on polymer substrates. Li_2MoO_4-based pastes with different amounts of $BaTiO_3$ were prepared to modify the dielectric properties of the films which resulted in changes in the electromagnetic characteristics of the capacitor. The research interest was to characterize and verify the material's electrical characteristics as a part of component properties, in contrast to large planar samples as studied in previous publications [10], [11].

This article is organized by presenting the low-temperature fabrication of capacitor structure and coating all-ceramic materials in Section II, followed by the theory for electrical characterization in Section III. Electromagnetic scattering parameter measurements of capacitor components are presented in Section IV, and through them, the permittivity of ceramic material coatings is finally characterized in Section V.

Two investigating microscopy methods were used in investigations: laser microscope (VK-X200, Keyence, Osaka, Japan) and field-emission scanning electron microscope (Ultra Plus, Zeiss, Karlsruhe, Germany). The electrical response of the capacitors was measured by a vector network analyzer (Agilent 8510C) from 45 MHz to 10 GHz. The component properties, such as capacitance and quality value, were

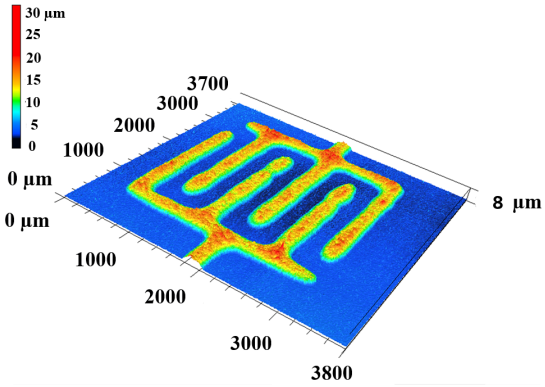

(a)

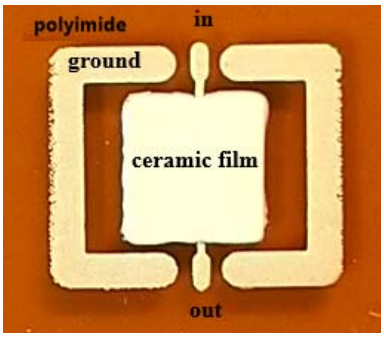

(b)

Fig. 1. (a) Laser microscopy image of silver printed six finger interdigital capacitor on polyimide substrate covering 2.5 × 2.5 mm area with linewidth of 250 μm. (b) Photograph of a measured interdigital capacitor component coated with 4 × 4 mm all-ceramic thick film. Polyimide film (dark brown) was used as a substrate with no ground below. The in and out ports are for 600-μm GSG probes. The ground lines locate around the capacitor making the maximum size of the component to be 8 × 7 mm.

calculated by mathematical formulas, and the material properties were extracted by simulations utilizing different curve fitting methods and assisted theoretical models, such as Debye, Lorenz, and Drude, which have not been compared earlier with this particular characterization method.

II. Experimental of Materials and Methods

A. Printing of the Uncoated Capacitors

Interdigital capacitor structures [Fig. 1(a) and (b)] with six pieces of 250-μm-wide fingers, each 1.7 mm in length, and 250-μm-wide insulating gaps between the fingers were printed on 125-μm-thick ε_r 3.5 loss tangent 0.009 (100 MHz) polyimide substrates (Kapton 500HN, Lohmann, Neuwied, Germany) (max T 400 °C) using a screen printer (MPM/SPM, Speedline Technologies, Franklin, MA) and silver conductor paste (5064H, DuPont, Wilmington, DE). Prior to the printing, the substrates were wiped clean of grease and dust with acetone. A total of 20 capacitor structures were printed, dried at 130 °C for 20 min, and their electromagnetic responses were measured.

B. Printing of Ceramic Thick Films

Development and preparation of the all-ceramic films using the RTF method was described in a recent paper [11]. The printable pastes were realized using Li_2MoO_4 and $BaTiO_3$

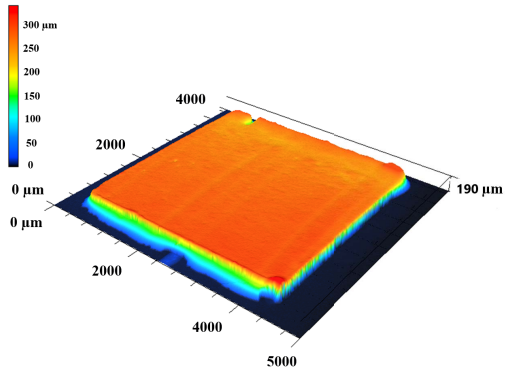

Fig. 2. Laser microscopy image of an interdigital capacitor on polyimide substrate coated with 190-μm-thick Sp.B composite film.

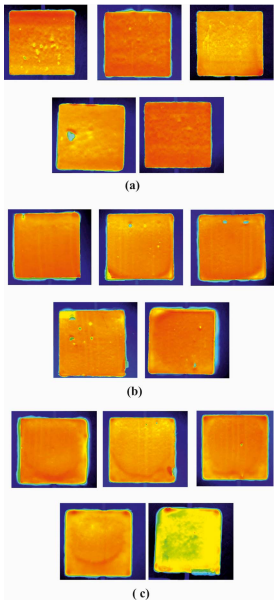

Fig. 3. Laser microscope images of the capacitors with all-ceramic $Li_2MoO_4/BaTiO_3$ coatings. (a) Five pieces of Sp.A, (b) five pieces of Sp.B, and (c) five pieces of printed Sp.C samples.

powders (0, 10, and 20 vol.% in relation to the amount of Li_2MoO_4) and deionized water. In this article, these compositions are denoted as follows:

Sp.A Li_2MoO_4
Sp.B $0.9Li_2MoO_4/0.1BaTiO_3$
Sp.C $0.8Li_2MoO_4/0.2BaTiO_3$.

The printing of the pastes on top of the capacitors was conducted manually using a rigid steel squeegee and a laser-cut steel stencil (thickness 100 μm) with an aperture size of 4 × 4 mm. The paste filled the gaps between the capacitor fingers. Double pass off-contact printing (gap 1 mm) with a 10-min waiting period between the strokes produced films with either zero or very few pinholes, as shown in Figs. 2 and 3. Five capacitors were coated using each type of material and the drying of the films followed the previous procedure [11] with a final treatment at 120 °C for 3 h to ensure complete drying [10]. Then, the electromagnetic responses of the samples were measured again. Therefore, every component supplied both uncoated and coated measurement results for further analysis.

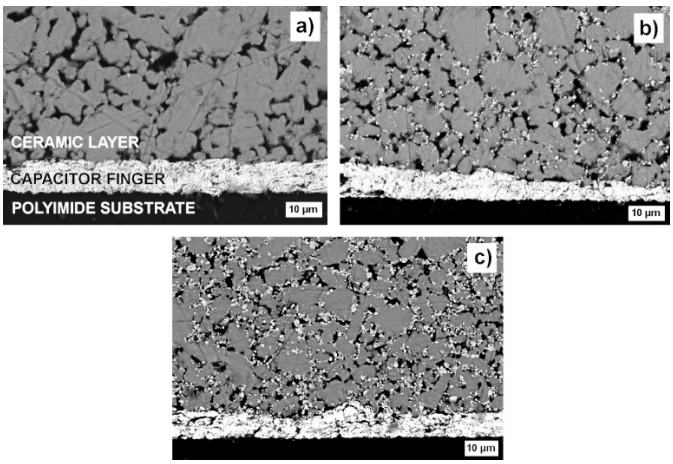

Fig. 4. Backscattered electron images of sample cross sections with (a) Sp.A, (b) Sp.B, and (c) Sp.C composite ceramic films. In the ceramic films, the gray particles denote Li_2MoO_4, small white particles denote $BaTiO_3$, and the black areas between the particles denote porosity, respectively.

C. Analysis and Characterization of the Ceramic Thick Films

The profiles of both the uncoated and coated capacitors were studied with a laser microscope using 10× magnification. The surface quality was the highest with Sp.C, as shown in Fig. 3(c), where there was the lowest mount of observed defects on the surface compared with the Sp.A and Sp.B, as shown in Fig. 3(a) and (b). The average thickness of the films was 160 μm (ranging from 130 to 190 μm), while relative density had previously been measured to be 66%–69% [11].

The microstructures of the sample cross sections were analyzed with a field-emission scanning electron microscope. The samples were cast in epoxy and the cross sections, perpendicular to the direction of capacitor fingers, were revealed by polishing with abrasive papers [11]. To eliminate the electrostatic effects during imaging, the samples were coated with a thin layer of carbon. The microstructures in Fig. 4 show seamless contacts between the polyimide substrate, the capacitor fingers, and the ceramic films. In addition, the two printed ceramic layers merged with each other without remarkable porosity or defects. These observations were in accordance with previous results [11], [12].

III. Electromagnetic Analysis of Measured Components and Materials

A. Parameter Formulas for Component Characterization

In the electromagnetic characterization, various methods were used for calculating the component properties, such as the capacitance and the quality value. Component measurement results were used together with other methods for calculating the material properties, such as the relative permittivity and the loss tangent, utilizing curve fitting methods.

For calculating the component properties, the measured scattering S-parameter results were converted into admittance Y-parameters by using the following formulas [7], [19]:

$$d = ((1 + S_{11})(1 + S_{22}) - S_{12}S_{21}) \quad (1)$$

$$Y_{11} = \frac{((1 - S_{11})(1 + S_{22}) - S_{12}S_{21})}{d} \quad (2)$$

$$Y_{22} = \frac{((1 + S_{11})(1 - S_{22}) - S_{12}S_{21})}{d} \quad (3)$$

$$Y_{12} = -2 * \frac{S_{12}}{d} \quad (4)$$

$$Y_{21} = -2 * \frac{S_{21}}{d}. \quad (5)$$

The component's quality value Q was calculated from the S-parameters using the equation

$$Q = \left| \frac{\mathrm{Im}(Y_{21})}{\mathrm{Re}(Y_{21})} \right| \quad (6)$$

where imaginary value of Y_{21} is divided by real value of Y_{21}, and the capacitance C from

$$C = \frac{10^{12}}{2\pi f * \mathrm{Im}\left(\frac{1}{Y_{21}}\right)} \text{ pF} \quad (7)$$

where f is the frequency.

B. Parameter Formulas for Material Characterization

The electromagnetic modeling of the capacitor component in terms of the various materials was realized by utilizing the curve fitting method, where the response of the 3-D simulation model (CST Microwave Studio) and the measurement results were compared with each other. Theoretical models of first- and second-order Debye, Lorenz, and Drude [20], [21] were evaluated for the calculation of the material permittivity characteristics over a large frequency range from 45 MHz to 10 GHz.

The first-order Debye material frequency dispersion model describes the relaxation process of a material, determined by the relaxation time and the epsilon static value. The second-order Debye dispersion describes a superposed relaxation process given by the summation of two separate first-order Debye models decreasing the scattering parameter variation of measured and simulated results as well as describing two different kind characteristics of materials used in the composite. They can be calculated by

$$\varepsilon_r(\omega) = \varepsilon'_\infty + \sum_i^n \frac{\varepsilon'_{si} - \varepsilon_\infty}{1 + j\omega\tau_i} \quad (8)$$

where ε'_∞ is the high-frequency permittivity, ε'_{si} and ε_∞ are static and infinity permittivity, τ_i is the characteristic relaxation time of the medium, and ω is the angular frequency.

The Drude dispersion model describes the dielectric behavior of plasma material, determined by the plasma frequency and the collision frequency representing damping effects

$$\varepsilon_r(\omega) = 1 - \frac{\omega_p^2}{\omega^2 + j\Gamma_d\omega} \quad (9)$$

where Γ_d and ω_p are oscillation restoring force and the angular frequency, respectively.

The Lorentz dispersion model describes a material resonance process, determined by the permittivity static value, the angular frequency, and the damping factor. Lorenz dispersion is calculated by:

$$\varepsilon_r(\omega) = \varepsilon'_\infty + \frac{(\varepsilon_{si} - \varepsilon_\infty)\omega_t^2}{\omega_t^2 - \omega^2 + j\Gamma_0\omega} \quad (10)$$

where ω_t is angular resonance frequency and Γ_0 is damping factor.

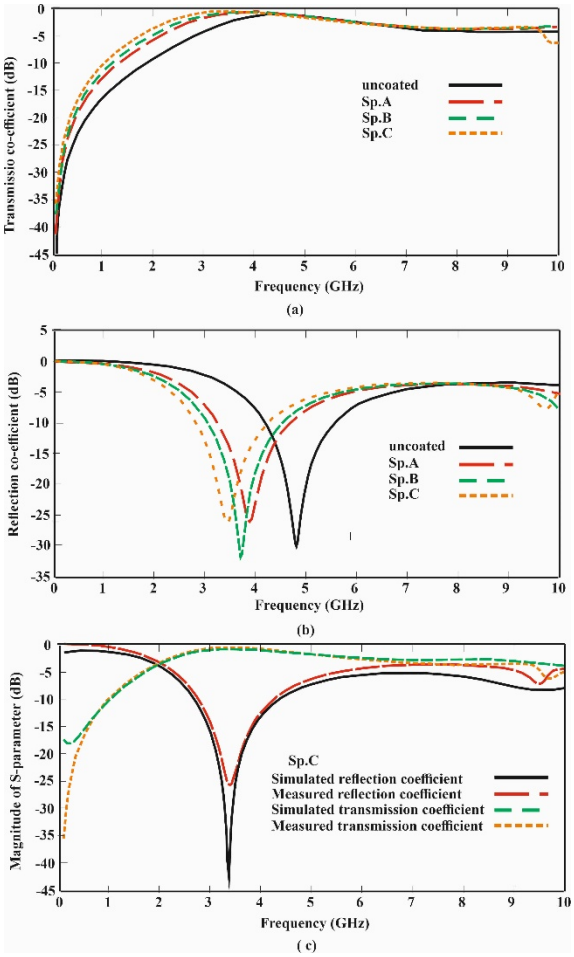

Fig. 5. Measurements performed from 45 MHz to 10 GHz. (a) Measured transmission coefficient of the uncoated capacitor, and coated with Sp.A, B, and C films. (b) Measured reflection coefficient of capacitor of the uncoated, and with Sp.A, B, and C films. (c) Comparison of simulated and measured S-parameter responses of Sp.C film capacitor.

IV. Measured Electromagnetic Properties of Capacitors

A. Scattering Parameter Results for Capacitors

Two-port S-parameters of the capacitors were measured by using the vector network analyzer, a probe station, and two 600-μm GSG probes, LRRM calibration method and a Cascade manufactured calibration substrate. The transmission and reflection coefficients of the capacitors were measured from 45 MHz to 10 GHz, and the results are presented in Fig. 5(a) and (b), and the simulation-measurement data comparison is shown in Fig. 5(c). The components behaved as a typical capacitor with small transmission coefficient at low frequencies and a high transmission coefficient at high frequencies. The transmission coefficient values were the highest between 3- and 5-GHz frequencies. The resonances

TABLE I
OVERALL STATISTICAL VALUES OF CAPACITORS MEASURED FROM FIVE CAPACITORS

Ceramic coating material	Average value of transmission attenuation at 2.5 GHz (dB)	Standard deviation value of transmission attenuation at 2.5 GHz (dB)	Average value of transmission attenuation at 9 GHz (dB)	Standard deviation value of transmission attenuation at 9 GHz (dB)
uncoated	-6.98	0.10	-3.98	0.02
Sp.A	-3.50	0.38	-3.89	0.12
Sp.B	-2.76	0.33	-3.62	0.15
Sp.C	-1.56	0.08	-3.51	0.08

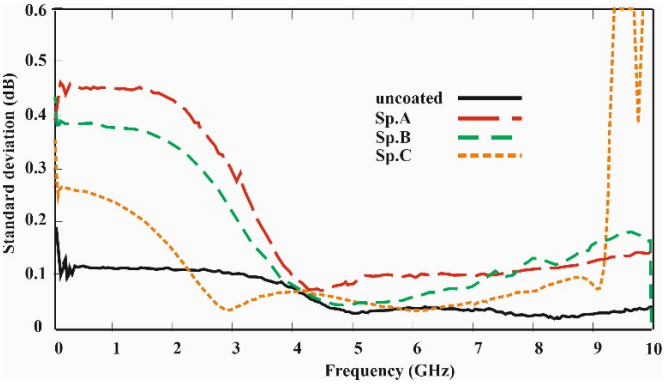

Fig. 6. Standard deviation of measurement results of transmission coefficient for capacitors with Sp.A, B, and C coatings.

with different ceramic are clearly presented in Fig. 5(b), where the characteristic self-resonances of the capacitor are observed by the minimum values of the reflection coefficient. The uncoated capacitor had its resonance at 4.9 GHz, with Sp.A at 4.0 GHz, with Sp.B at 3.8 GHz, and with Sp.C at 3.4 GHz, where the transmission coefficients were at their maximum and the reflection coefficients were at their minimum values, respectively.

B. Statistics of Measurement Results

The overall statistical values of the capacitors were evaluated from the measurement results by calculating the average transmission coefficient values and the standard deviation values at 2.5 and 9 GHz from five pieces of particular samples (Table I). Notably, 2.5 GHz is widely used telecommunication radio band and 9 GHz corresponds to earlier published material measurement results [10], [11]. The standard deviation of the measurement results for entire frequency band is presented in Fig. 6. These parameters describe how much the electrical response varied due to the fabrication and material tolerances over the frequency range. The standard deviation values calculated at a point frequency of 2.5 GHz were 0.12, 0.38, 0.33, and 0.08 dB for uncoated, Sp.A, Sp.B, and Sp.C samples, and the standard deviation values calculated at a point frequency of 9 GHz were 0.02, 0.12, 0.20, and 0.08 dB, respectively. The deviation had larger values at low frequencies from 45 MHz to 4 GHz than at frequencies from 4 GHz to 10 GHz. The ceramic film with the highest $BaTiO_3$ content, i.e., Sp.C, had the smallest variation in the measurement results.

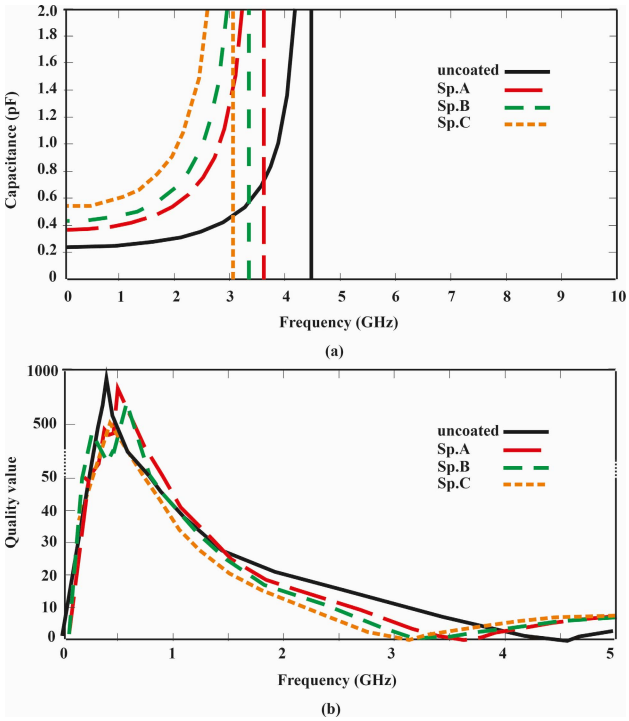

Fig. 7. Measured equivalent capacitance and quality values. (a) Capacitance with uncoated, Sp.A, B, and C films. (b) Quality value with uncoated, Sp.A, B, and C films.

C. Capacitance and Quality Value Calculations

The capacitance and quality values of capacitors were calculated by (1)–(7) as presented in [6]. The capacitance values of capacitors without and with different coatings in terms of the frequency are presented in Fig. 7(a). Uncoated, Sp.A, Sp.B, and Sp.C, capacitance values started from 0.23, 0.35, 0.43, and 0.53 pF at 45 MHz increases toward the maximum value at 4.5, 3.6, 3.25, and 3.05 GHz, respectively. The capacitance per area values was 0.04, 0.06, 0.07, and 0.08 pF/mm^2, and they increased by 50%, 75%, and 100% for the measured materials. Quality values of capacitors are presented in Fig. 7(b). The quality values were over 50 in the 45-MHz to 1-GHz frequency range, decreasing to 10–20 at 2 GHz. The ceramic coatings on the capacitor decreased the self-resonance frequency, increased the capacitance, and decreased the quality value, as expected.

The studied capacitor structure had 0.36-pF uncoated capacitance with the ceramic coatings 0.75-, 1.03-, and 1.73-pF

capacitance (Sp.A, B, and C) at 2.5 GHz. The component's optimum frequency range in radio applications was within the 1–5-GHz frequency band, and it was working on inductive characteristics over 5 GHz. The second-order resonance was not seen until 10 GHz, which was the highest measurement frequency. At 2.5 GHz, the capacitance per area was 0.06, 0.12, 0.16, and 0.28 pF/mm^2 (uncoated, Sp.A, B, and C) increasing relatively with added materials by 100%, 167%, and 367%. The quality values at 2.5 GHz for the whole component were 20, 18, 17, and 15 at 2 GHz, respectively.

V. Extraction of Material Permittivity Values From Component Measurements

A. Procedure for Material Parameter Characterization

The extraction of the real and imaginary permittivity values of coating materials was conducted using the following steps.

1) Two-port *S*-parameter response of the uncoated capacitance sample #n was measured from 45 MHz to 10 GHz.
2) Three-dimensional simulation model of sample #n was built, and corresponding conductor- and substrate-related material and dimensional parameters were simulated.
3) Ceramic coating Sp.A, B, or C was printed on the sample #n and corresponding *S*-parameters were measured.
4) Parameters related to the printed ceramic coating (Sp.A, B, or C) were simulated by using 3-D simulation model for sample #n.

Parameters calculated in step 2 were not changed later in step 4. Step 4 is optimized by adjusting the position of the self-resonance frequency and the level of transmission coefficient of the capacitor between the measured and simulated results.

B. Accuracy of Measurements and Modeling

The overall accuracy between the 3-D simulation model of the capacitance and the measurement results was a maximum of 0.05 in the linear scale of the transmission *S*-parameters over the measured frequency band from 45 MHz to 10 GHz. The inaccuracy related to the wideband simulation model was larger than the standard deviation in the measurements. By using the previous material extraction procedure, the overall accuracy of the 3-D simulation model of the material against the measurement results was a maximum of 0.01 in the linear scale of the transmission *S*-parameter calculated at point frequencies 2.5 and 9 GHz. This accuracy of result was clearly higher than the measured standard deviation in the fabrication. The characterized resonance position of the frequency was very accurate, and it improved the overall accuracy of the material characterization. Further calculated tolerances were 0.01 for the real value of the relative permittivity and 0.01 for the loss tangent of the ceramic coatings. In this characterization, the accuracy of loss tangent extraction was limited mainly by the tolerances of the manual measurements and the variable contact resistance of the GSG probes between measured samples.

C. Material Permittivity Calculation Results

Simulated real and imaginary permittivity values of Sp.A material calculated using (8)–(10), models of first- and second-order Debye, Lorenz, and Drude models are presented in Fig. 8. With the first-order Debye model, the real and imaginary permittivity values were 5.2 and 0.77 at 500 MHz. With the Lorenz, second-order Debye, and Drude models, the corresponding parameters were 4.73, 4.65, 3.65, and 0.6, 0.53, 0.05. The first-order Debye had the highest value, the second-order Debye and Lorenz models had values close to each other, and the Drude model produced the lowest values. The first-order Debye calculated values were the closest to the split-post-resonator results in Väätäjä *et al.* [11].

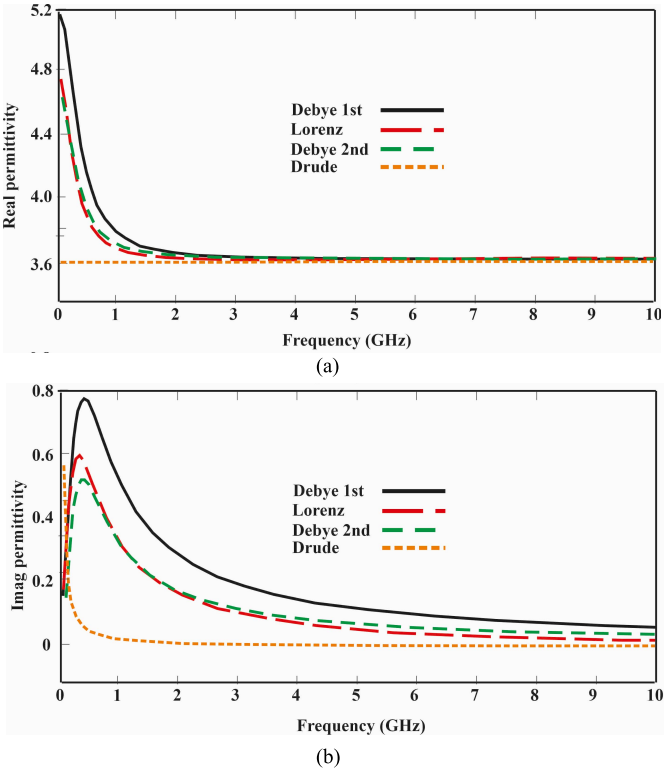

Fig. 8. (a) Simulated material real permittivity and (b) simulated material imaginary permittivity value of Sp.A based on first-order Debye, Lorenz, second-order Debye, and Drude models.

By applying the first-order Debye model, all sample material parameters were calculated by CST software utilizing (8), and the resulting real and imaginary permittivity values are presented in Fig. 9. Material values were used as variables in the simulations. The real and imaginary values for Sp.A material were 3.72 and 0.13, that for Sp.B material was 5.25 and 0.14, that for Sp.C material was 6.45 and 0.23 at 2.5-GHz frequency, respectively. The results are collected in Table II. High-frequency real values were almost the same, but smaller imaginary values produced smaller loss tangents at 9 GHz. Extracted loss tangents were 0.035, 0.027, and 0.036 at 2.5 GHz and 0.010, 0.009, and 0.009 at 9 GHz for Sp.A, Sp.B, and Sp.C materials. Applying other models, such as the Lorenz model, the loss tangents at 9 GHz were lower: 0.003, 0.003, and 0.002 for Sp.A, B, and C materials, respectively. The accuracy of the real permittivity values was ±0.01 and that of the loss tangent was ±0.01 calculated from simulation accuracy. The loss tangent characterized values were on the model accuracy limit, and there was no trend seen despite the different $BaTiO_3$ contents of the materials at 9 GHz. The

TABLE II
PROPERTIES OF THE CERAMIC FILMS

Ceramic coating material	Simulated real permittivity at 2.5 GHz	Simulated imaginary permittivity at 2.5 GHz	Simulated real permittivity at 9 GHz	Simulated imaginary permittivity at 9 GHz	Loss tangent at 2.5 GHz	Loss tangent Debye1 at 9 GHz	Loss tangent Debye2 at 9 GHz	Loss tangent Lorenz at 9 GHz	Loss tangent Drude at 9 GHz
Sp.A	3.72	0.13	3.70	0.038	0.035	0.010	0.006	0.003	0.0005
Sp.B	5.25	0.14	5.23	0.049	0.027	0.009	0.006	0.003	0.0005
Sp.C	6.45	0.23	6.43	0.056	0.036	0.009	0.005	0.002	0.0004

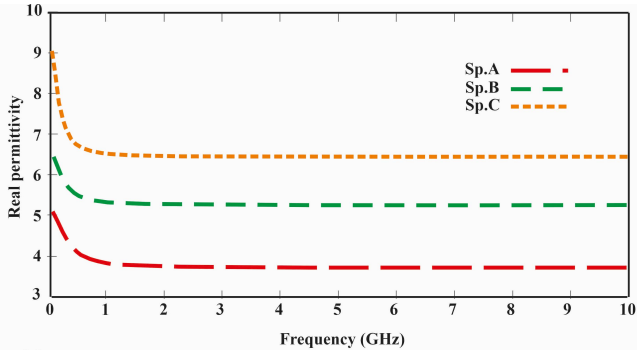

(a)

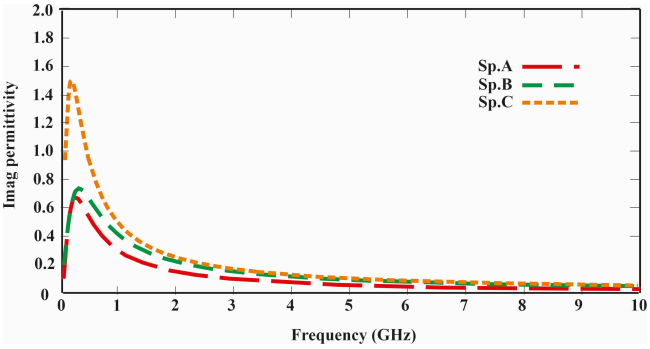

(b)

Fig. 9. (a) Simulated material real permittivity and (b) simulated material imaginary permittivity of Sp.A, Sp.B, and Sp.C films.

accuracy of real permittivity and the loss tangent values was limited by the contact resistance tolerances that were 0.01 in the linear scale of *S*-parameters, i.e., 0.06 dB at 2.5 GHz, which was more accurate than the fabrication tolerances. The problem with other permittivity characterization methods is that the thickness, count of print layers, total volume, and other details vary between the material sample and the realized component. In general, fabrication tolerances of printed electronics technology could be over 5%–10% between components that constantly complicates the design process and even more so in the future when the frequency is increased, for example, in 5G and 6G telecom systems and when fabrication methods change, e.g., in printed electronics.

In [11], the dielectric properties of the ceramic films, measured using dielectric split post resonators at 2.5 GHz, were found to be (ε_r/tanδ) 4.2 ± 0.3/0.005, 6.1 ± 0.4/0.012, and 7.2 ± 0.3/0.022. At 9.9 GHz, the values were 4.5 ± 0.6/0.001, 6.6 ± 0.3/0.011, and 7.5 ± 0.6/0.022. Compared with these results, the Sp.A simulated value of 3.72 was 10% lower, Sp.B simulated value of 5.25 was 14% lower, and Sp.C simulated value of 6.45 was 10% lower. In [11], the measured samples were realized with a single-printed layer with average thickness of 73 μm, whereas in this article, two printed layers and on average 160-μm film thickness were used. The results follow the observation in [19], where by increasing the number of print layers, the material's relative permittivity decreased. The relative permittivity of Li_2MoO_4 was measured at 9 GHz to be 5.1 in [10], 4.5 in [11], and 3.72 in this article, thus highlighting the effect of the fabrication process and the consequent realized material properties in the final component. The material characterization method used in this article was valid for relative permittivity measurement for the capacitor but invalid for accurate loss tangent measurements. Instead, the material loss characterization should be realized by the split-post resonator method.

VI. CONCLUSION

This article presents the characterization of electromagnetic properties of printed all-ceramic composites, Li_2MoO4, $0.9Li_2MoO_4/0.1BaTiO_3$, and $0.8Li_2MoO_4/0.2BaTiO_3$, by measuring and simulating an interdigital capacito component coated with these three different composite films.

The real permittivity and loss tangent values for Li2MoO4 film were 3.72/0.035, for $0.9Li_2MoO_4/0.1BaTiO_3$ 5.25/0.027 and for $0.8Li_2MoO_4/0.2BaTiO_3$6.45/0.036 at 2.5-GHz frequency.

In material parameter calculations, Lorenz, first- and second-order Debye, and Drude models were compared. The first-order Debye calculated permittivity results were the closest for the results achieved previously by the split-post-resonators [11].

The printed all-ceramic $Li_2MoO_4/BaTiO_3$ composite films are competitive dielectrics for high-frequency applications at 45 MHz to 10 GHz. The permittivity and loss tangent values are comparable with the corresponding values measured previously from polymer–ceramic composites [4]–[8] extending the opportunities of material selections within the roadmap of high-temperature resistant material for printed electronics and 5G telecommunications [9] technologies.

ACKNOWLEDGMENT

Maciej Sobocinski and Jaakko Palosaari are acknowledged for their assistance in screen printing of the capacitors and laser cutting of the stencil, respectively. The Materials and Mechanical Engineering Research Unit, University of Oulu, Oulu, Finland, is acknowledged for the use of the laser microscope.

M.Väätäjä gratefully acknowledges Infotech Oulu Doctoral Program, the Finnish Foundation for Technology Promotion, the Riitta and Jorma J. Takanen Foundation, the Walter Ahlström Foundation, and the Tauno Tönning Foundation.

REFERENCES

[1] J. S. Chang, A. F. Facchetti, and R. Reuss, "A circuits and systems perspective of organic/printed electronics: Review, challenges, and contemporary and emerging design approaches," *IEEE J. Emerg. Sel. Topics Circuits Syst.*, vol. 7, no. 1, pp. 7–26, Mar. 2017.

[2] Y. Khan, A. Thielens, S. Muin, J. Ting, C. Baumbauer, and A. C. Arias, "A new frontier of printed electronics: Flexible hybrid electronics," *Adv. Mater.*, vol. 32, no. 15, Nov. 2019, Art. no. 1905279.

[3] M. Nelo, A. Sowpati, V. K. Palukuru, J. Juuti, and H. Jantunen, "Formulation of screen printable cobalt nanoparticle ink for high frequency applications," *Prog. Electromagn. Res.*, vol. 110, pp. 253–266, 2010.

[4] S.-H. Xie, B.-K. Zhu, X.-Z. Wei, Z.-K. Xu, and Y.-Y. Xu, "Polyimide/$BaTiO_3$ composites with controllable dielectric properties," *Compos. A, Appl. Sci. Manuf.*, vol. 36, no. 8, pp. 1152–1157, Aug. 2005.

[5] J. Chameswary and M. T. Sebastian, "Preparation and properties of $BaTiO_3$ filled butyl rubber composites for flexible electronic circuit applications," *J. Mater. Sci., Mater. Electron.*, vol. 26, no. 7, pp. 4629–4637, Feb. 2015.

[6] O. Gbotemi *et al.*, "Characterization of PMMA/$BaTiO_3$ composite layers through printed capacitor structures for microwave frequency applications," *IEEE Trans. Microw. Theory Techn.*, vol. 66, no. 4, pp. 1736–1743, Apr. 2018.

[7] S.-F. Wang, Y.-R. Wang, K.-C. Cheng, and Y.-P. Hsaio, "Characteristics of polyimide/barium titanate composite films," *Ceram. Int.*, vol. 35, no. 1, pp. 265–268, Jan. 2009.

[8] M. Mikolajek *et al.*, "Fabrication and characterization of fully inkjet printed capacitors based on ceramic/polymer composite dielectrics on flexible substrates," *Sc. Rep.*, vol. 9, Sep. 2019, Art. no. 13324.

[9] I. Ndip and K.-D. Lang, "Roles and requirements of electronic packaging in 5G," in *Proc. 7th Electron. Syst.-Integr. Technol. Conf. (ESTC)*, Dresden, Germany, Sep. 2018, pp. 1–5.

[10] H. Kähäri *et al.*, "Improvements and modifications to room-temperature fabrication method for dielectric Li_2MoO_4 ceramics," *J. Amer. Cer. Soc.*, vol. 98, no. 3, pp. 687–689, 2015.

[11] M. Väätäjä, H. Kähäri, K. Ohenoja, J. Juuti, and H. Jantunen, "Direct integration of dielectric all-ceramic thick films on a polymer substrate using room temperature fabrication," *J. Eur. Ceram. Soc.*, vol. 40, no. 12, pp. 3984–3988, Sep. 2020.

[12] M. Vätäjä *et al.*, "3D printed dielectric ceramic without a sintering stage," *Sc. Rep.*, vol. 8, Oct. 2018, Art. no. 15955.

[13] M. N. Afsar, J. R. Birch, R. N. Clarke, and G. W. Chantry, "The measurement of the properties of materials," *Proc. IEEE*, vol. 74, no. 1, pp. 183–199, Jan. 1986.

[14] R. J. Cook, "Microwave cavity methods," in *High Frequency Dielectric Measurement*, J. Chamberlain and G. W. Chantry, Eds. Guildford, U.K.: IPC Science and Technology, 1973, pp. 12–17.

[15] M. A. Stuchly and S. S. Stuchly, "Coaxial line reflection method for measuring dielectric properties of biological substances at radio and microwave frequencies—A review," *IEEE Trans. Instr. Meas.*, vol. IM-29, no. 3, pp. 176–183, Sep. 1980.

[16] D. K. Ghodgaonkar, V. V. Varadan, and V. K. Varadan, "Free-space measurement of complex permittivity and complex permeability of magnetic materials at microwave frequencies," *IEEE Trans. Instrum. Meas.*, vol. 39, no. 2, pp. 387–394, Apr. 1990.

[17] A.-H. Boughriet, C. Legrand, and A. Chapoton, "Noniterative stable transmission/reflection method for low-loss material complex permittivity determination," *IEEE Trans. Microw. Theory Techn.*, vol. 45, no. 1, pp. 52–57, Jan. 1997.

[18] M. Nelo, S. Myllymäki, J. Juuti, A. Uusimäki, and H. Jantunen, "Cobalt nanoparticle inks for printed high frequency applications on polycarbonate," *J. Electron. Mater.*, vol. 44, no. 12, pp. 4884–4890, Dec. 2015.

[19] T. Bluhm. (2001). *S-Parameters—Characteristics of Passive Components, BC Components, Technical Note*. [Online]. Available: https://www.ieee.li/pdf/essay/s_parameters_of_passive_components.pdf

[20] N. S. Stoykov, T. A. Kuiken, M. M. Lowery, and A. Taflove, "Finite-element time-domain algorithms for modeling linear Debye and Lorentz dielectric dispersions at low frequencies," *IEEE Trans. Biomed. Eng.*, vol. 50, no. 9, pp. 1100–1107, Sep. 2003.

[21] Material Overview (HF). (2018). *CST Microwave Studio*. [Online]. Available: http://www.mweda.com/cst/cst2013/mergedprojects/CST_MICROWAVE_STUDIO/special_overview/special_overview_material_overview_hf.htm

S. Myllymäki received the M.Sc. and D.Sc. degrees from the University of Oulu, Oulu, Finland, in 1999 and 2012, respectively.

He is currently a Research Group Leader and an Adjunct Professor with the Microelectronics Research Unit. His interests are microwave measurements, components, materials, and electronics packaging technology.

M. Väätäjä received the M.Sc. degree in inorganic chemistry from the University of Oulu, Oulu, Finland, in 2015, where she is currently pursuing the Ph.D. degree with the Microelectronics Research Unit.

Her research interests include low-temperature manufacturing of electroceramics and ceramic composites.

G. Omodara is currently pursuing the Ph.D. degree with the Microelectronics Research Unit, University of Oulu, Oulu, Finland.

His current research interests include antennas, electronic materials, and passive components for RF and microwave applications.

H. Kähäri received the D.Sc. degree from the University of Oulu, Oulu, Finland, in 2016.

She is a Technical Leader (materials) with Nokia Corporation, Espoo, Finland.

J. Juuti received the D.Sc. degree from the University of Oulu in 2006.

He joined as a Docent/Adjunct Professor in 2009. He is currently an Academy Research Fellow with the Academy of Finland. His current research interests include piezoelectrics and functional composites for telecom and printed electronics.

H. Jantunen received the D.Sc. degree from the University of Oulu in 2001.

She is a Professor in technical physics and a Leader with the Microelectronics Research Unit, Faculty of Information Technology and Electrical Engineering, University of Oulu, Oulu, Finland. Her research areas cover novel functional materials enabling advanced devices for ICT application with low-temperature fabrication and printed or injection molding methods.